JACS
JOURNAL OF THE AMERICAN CHEMICAL SOCIETY
Article
pubs.acs.org/JACS

High Oxidation State Iridium Mono-μ-oxo Dimers Related to Water Oxidation Catalysis

Liam S. Sharninghausen,[‡,⊥] Shashi Bhushan Sinha,[‡,⊥] Dimitar Y. Shopov,[‡,⊥] Bonnie Choi,[†] Brandon Q. Mercado,[⊥] Xavier Roy,[†] David Balcells,[*,§] Gary W. Brudvig,[*,⊥] and Robert H. Crabtree[*,⊥]

[⊥]Department of Chemistry, Yale University, New Haven, Connecticut 06520, United States

[†]Department of Chemistry, Columbia University, New York, New York 10027, United States

[§]Centre of Excellence in Theoretical and Computational Chemistry, Department of Chemistry, University of Oslo, N-0315 Oslo, Norway

Supporting Information

ABSTRACT: The highly active iridium "blue solution" chemical and electrochemical water oxidation catalyst obtained from Cp*IrL(OH) precursors (L = 2-pyridyl-2-propanoate) has been difficult to characterize as no crystal structure can be obtained because of the multiplicity of geometrical isomers present. Other data suggest complete loss of the Cp* ligand and the formation of a LIr-O-IrL unit. We have now developed a route to a series of well-defined Ir(IV,IV) mono-μ-oxo dimers, containing the closely related L_2Ir-O-IrL_2 unit. Unlike the catalyst, these model compounds are separable by silica gel chromatography and readily form single crystals. We report three stereoisomers with the formula ClL_2Ir-O-IrL_2Cl, which are fully characterized, including by X-ray crystallography, and are compared to the "blue solution". To the best of our knowledge, these species represent the first examples of structurally characterized dinuclear μ-oxo Ir(IV,IV) compounds without metal−carbon bonds.

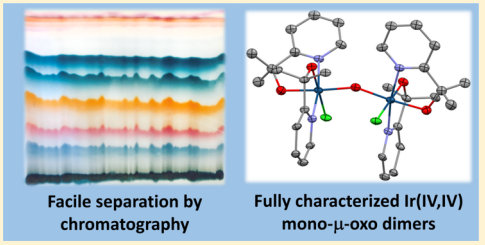

INTRODUCTION

Interest in water oxidation (WO) catalysis has grown considerably in recent years in connection with the rise in global demand for renewable energy.[1] Water oxidation is an endergonic four-electron process with a standard reduction potential of 1.23 V, which in practice, however, requires a large additional overpotential to drive the kinetics. Design and study of catalysts is, therefore, needed to make this reaction as efficient as possible by lowering the energy demands.[2] Owing to the harsh oxidizing conditions required for WO, most current ligands are oxidatively degraded during the reaction.[3] In 2009, our group reported a series of Cp*Ir chelate (Cp* = pentamethylcyclopentadienyl) precatalysts for WO,[4] and since then this class of complexes has been extensively investigated by us and others.[5] Spectroscopic studies showed that the Cp* ligand is gradually lost through oxidative degradation when Cp*Ir WO precatalysts are exposed to the reaction conditions.[6] In the presence of oxidation-resistant chelate ligands, this process results in homogeneous and catalytically active solutions with an intense blue color.[7] The most active catalytic mixture is obtained from the precatalyst Cp*Ir(pyalk)OH with 2-pyridyl-2-propanoate (pyalk) as the chelating ligand (Scheme 1). After Cp* loss, the resulting "blue solution" retains the pyalk ligand and is a robust and highly efficient WO catalyst (WOC), driven both electrochemically and chemically.[8] The pyalk ligand resists oxidative degradation due to the $-CMe_2$ group at the benzylic position and is also a powerful electron donor through its tertiary alkoxide, allowing Ir to access high oxidation states. This combination of electron donation and oxidation resistance makes pyalk a particularly suitable ligand for WO catalysis.[9]

Scheme 1. Preparation of "Blue Solution" by Oxidative Activation of Cp*Ir(pyalk)OH Precatalysts

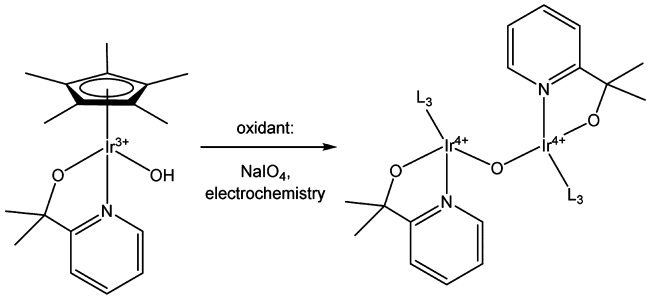

In previous work, we probed the chemical identity of the catalytically active Ir "blue solution" described above. An Ir(IV,IV) oxo dimer with one pyalk per Ir was proposed as the catalyst resting state based on extensive spectroscopic studies.[10] Although the spectroscopic data were originally interpreted in terms of a bis-μ-oxo Ir(IV,IV) "diamond core",[10] recent

Received: July 26, 2016
Published: November 15, 2016

DOI: 10.1021/jacs.6b07716
J. Am. Chem. Soc. 2016, 138, 15917−15926

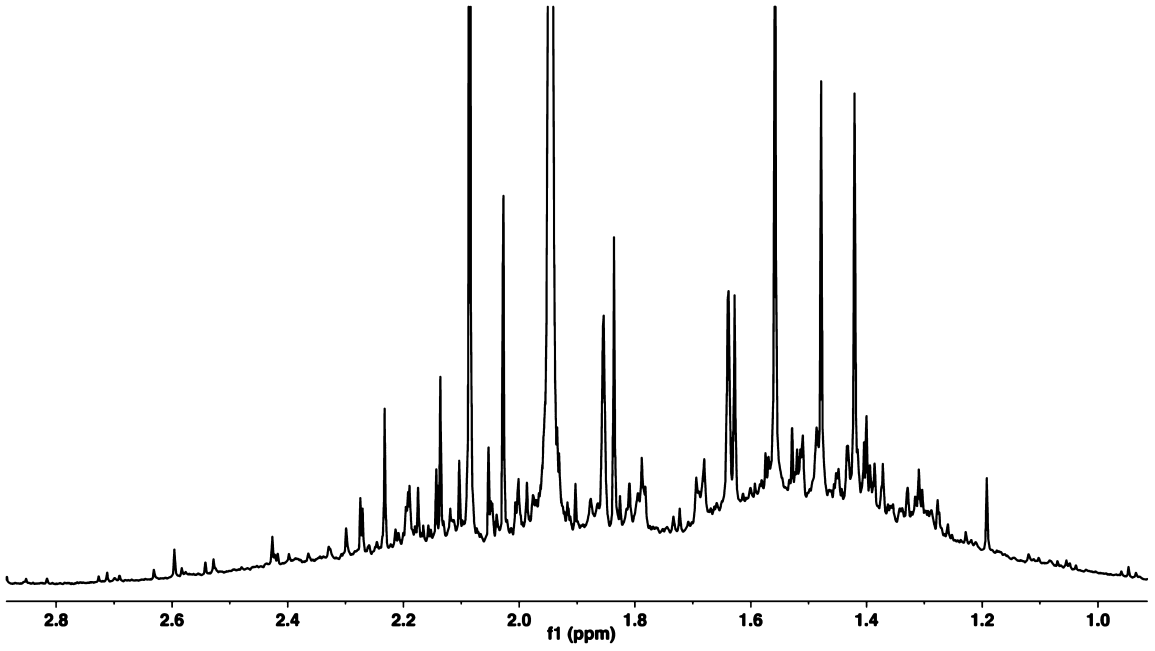

Figure 1. ^{1}H NMR of "blue solution" aliphatic region showing presence of multiple species. The large peak at ca. 1.95 ppm is from free acetate.

EXAFS, HEXS, and DFT work by Batista and co-workers[11] led to a mono-μ-oxo Ir(IV,IV) structure being preferred. The authors demonstrated that Raman data previously collected on the "blue solution" are more consistent with a mono-μ-oxo core, and that the Ir−Ir separation obtained by EXAFS was inconsistent with a "diamond-core" structure.[11] In addition, ^{17}O NMR spectra, which we previously interpreted as evidence for a di-μ-oxo structure, are ambiguous since ^{17}O NMR peak assignments are not well established.[10] However, despite extensive work on this system, the structural identity of the "blue solution" has remained uncertain because none of the proposed structures have been isolated or characterized by X-ray crystallography.

Recent work suggests that the "blue solution" is not a single compound but rather a mixture of closely related species and their geometrical isomers. For example, ^{1}H NMR spectra of these solutions display dense clusters of ligand peaks (Figure 1).[12] A likely explanation for this multiplicity comes from our previous finding that $Ir^{IV}(pyalk)_2Cl_2$ and $Ir^{IV}(pyalk)_3$ species are highly inert, and all possible geometrical isomers can exist without interconversion despite large differences in free energy, even at temperatures exceeding 100 °C.[9a,13] Furthermore, an even larger number of isomers is possible for the dinuclear (pyalk)Ir−O−Ir(pyalk) core. When this is combined with the fact that remaining sites may be occupied by water, acetate, or other auxiliary ligands formed in situ,[10−12] there can be myriad possible distinct structures (Scheme 1). The activity of the "blue solution" may thus arise from only a subset of the isomers, which have electronic and structural properties best suited for WO catalysis. However, attempts to separate the "blue solution" isomers using standard methods such as numerous types of chromatography have failed, and all crystallization attempts have proven unsuccessful. We previously found that the "blue solution" tenaciously binds to metal oxide surfaces through aqua sites, which is likely preventing chromatographic separation.[14]

Because of the problems associated with separating and characterizing the species present in the "blue solution", exploring related Ir(IV,IV) oxo-bridged dimers that can be isolated and structurally characterized is highly desirable. To our knowledge, there are only two reported examples of well characterized Ir(IV,IV) oxo dimers.[15] Iridium (IV,IV) bis-μ-oxo dimers have been proposed several times but have never been fully characterized.[16] Of course, a diamond core Ir_2O_2 motif is present in crystalline IrO_2, but with the binding of a third Ir atom to each oxo.[17] The two previously reported Ir(IV,IV)-mono-μ-oxo dimers are transient organometallic complexes containing alkyl or aryl ligands and are only stable at low temperature.[15] Because Ir(IV,IV) mono-μ-oxo dimers are relatively unexplored and no "classic" coordination complexes have been reported, we were interested in preparing such species with the pyalk ligand as models for the "blue solution". These could give insight into the structure of the latter, could facilitate elucidating the mechanism of Ir WO catalysis, and could be a starting point for the design of highly active Ir WOCs. Similar studies on Ru mono-μ-oxo-dimers indeed gave insight into the catalytic mechanism and led to the development of well-characterized WOCs.[18]

We recently synthesized and isolated a series of $Ir(pyalk)_2Cl_2$ isomers[13] that we thought would give access to specific μ-oxo dimers through substitution of the chloride ligands. Without the auxiliary ligand variability of the "blue solution", the number of possible mono-μ-oxo dimer products reduces from hundreds to about a dozen. Starting from a single $Ir(pyalk)_2Cl_2$ isomer, this number reduces to 1−6 possible species, assuming preservation of the monomer geometry. These dimers would resemble the proposed "blue solution" structure, but contain two pyalk ligands per Ir rather than one. The additional pyalk ligand should reduce the dimers' polarity as well as cut down on direct binding to silica, facilitating chromatographic separation.

We now report the successful synthesis, isolation, and characterization of three stable Ir(IV,IV) mono-μ-oxo dimers that appear to be the first of their kind. These complexes serve as models for the "blue solution" resting state, in line with the recent proposal by Batista and co-workers of an Ir mono-μ-oxo dimer structure.[11] While previous reports of Ir(IV) oxo dimers,

DOI: 10.1021/jacs.6b07716
J. Am. Chem. Soc. 2016, 138, 15917−15926

Scheme 2. General Preparation of Oxo Dimers

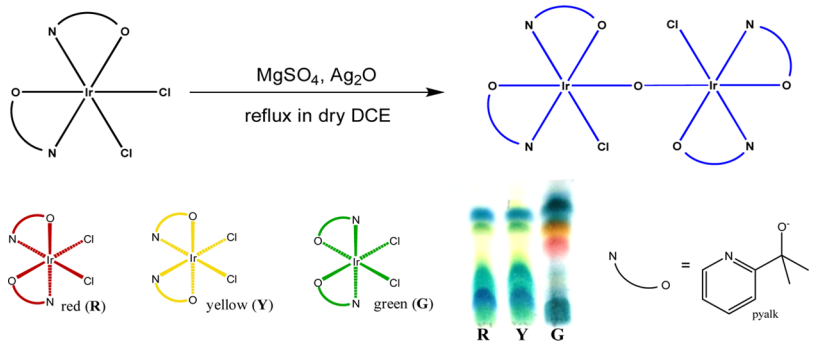

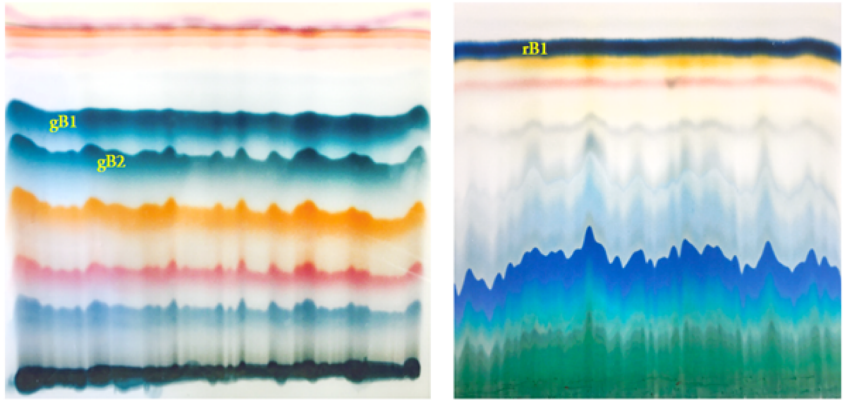

Figure 2. Preparative TLC separation of the coupling reaction products from **G** (left) and **R** (right) after elution with an acetone/water solution. Characterized blue species **gB1**, **gB2**, and **rB1** are labeled.

such as the "blue solution", typically involve spontaneous and nonselective dimerization, we offer the first synthetic protocol which allows for selectively forming and isolating geometrically defined Ir(IV,IV) mono-μ-oxo dimers.

RESULTS AND DISCUSSION

Preparation of Iridium(IV,IV) Oxo Species. Because all the possible geometrical isomers of $Ir^{IV}(pyalk)_2Cl_2$ can be obtained in pure form, we attempted to couple specific monomers to give specific mono-μ-oxo dimer isomers. Pure monomers were heated in refluxing dichloroethane under anhydrous conditions with Ag_2O as chloride abstractor and oxide source. Interestingly, we found that only those starting isomers containing *cis*-$IrCl_2$ units react with Ag_2O to form dinuclear complexes. These are the green (**G**), red (**R**), and yellow (**Y**) mononuclear isomers (Scheme 2). Moreover, the product mixtures arising from **Y** and **R** appear virtually identical chromatographically. We suspect this to be a result of two effects. One, isomerization can proceed at the reaction temperature, and we had previously observed that **Y** and **R** are sufficiently close in energy to coexist at thermodynamic equilibrium.[13] Two, the species we have so far been able to characterize (see below) all have alkoxide ligands *trans* to the oxo bridge. This may mean that the chloride ligand can only be abstracted by Ag_2O when there is sufficient *trans* activation by an O donor. Because **Y** has no chloride ligands trans to alkoxide, it may not be able to undergo dimerization until it has isomerized to **R**, which does have an alkoxide trans to Cl. In this paper, we focus only on the reactions using pure **R** and **G**, since **R** is the most abundant isomer and both **R** and **G** gave distinct and separable products (Figure 2). We found that high yields of the dinuclear species were observed only when aliquots of insoluble Ag_2O were added at regular intervals throughout the reaction. The optimal reaction time varies from 5 min for **R** to ~20 min for **G**.

An efficient separation procedure was needed to isolate the products of the coupling reactions. Silica gel column chromatography was not feasible because the polar nature of the products necessitates use of a partially aqueous eluent, yet isolation of pure species required a fairly high separation efficiency; we found the combination of these requirements impossible to achieve. We turned to preparative thin-layer silica gel chromatography (preparative TLC), which performed remarkably well under our conditions. Separation of the crude reaction mixtures using 5−10% water in acetone gives clean separation of the major blue species obtained from both reactions (Figure 2) and can be performed on a scale of up to 100 mg per plate with a 500 μm thick preparative TLC plate. Two discrete species derived from **G**, **gB1**, and **gB2** (named for their parent compound color, green (g), their blue color (B), and the order of elution), are stable in air at room temperature, while a blue species derived from **R**, **rB1**, is stable in the solid form but shows slow reductive degradation in solvent or on silica. These compounds exhibit a very broad solubility range, dissolving in solvents ranging from toluene to water and precipitating only in alkanes. This solubility is likely attributable to the amphiphilic properties of the pyalk ligand and is in contrast to the highly hydrophilic behavior of the species in the "blue solution", which bear half as many pyalk ligands. After optimization, we were able to obtain modest isolated yields of **gB1**, **gB2**, and **rB1** (22%, 7%, and 9%, respectively), facilitating further characterization.

DOI: 10.1021/jacs.6b07716
J. Am. Chem. Soc. 2016, 138, 15917−15926

High-resolution mass spectrometry (HRMS) of all three blue species gives nearly identical mass and isotope distributions (Figures S4–S6), consistent with Ir mono-μ-oxo dimers with two pyalk ligands and one chloride per iridium atom. As with the monomers, these dimers exhibit coordination inertness, as no isomerization is observed in pure samples kept at room temperature. This further supports the hypothesis that the "blue solution" can contain a nonequilibrium mixture of inert isomers.

Crystals were grown of all three compounds, and X-ray diffraction supports their assignment as Ir(IV,IV) mono-μ-oxo dimers (Figure 3). Bond lengths to Ir (Table 1) are consistent

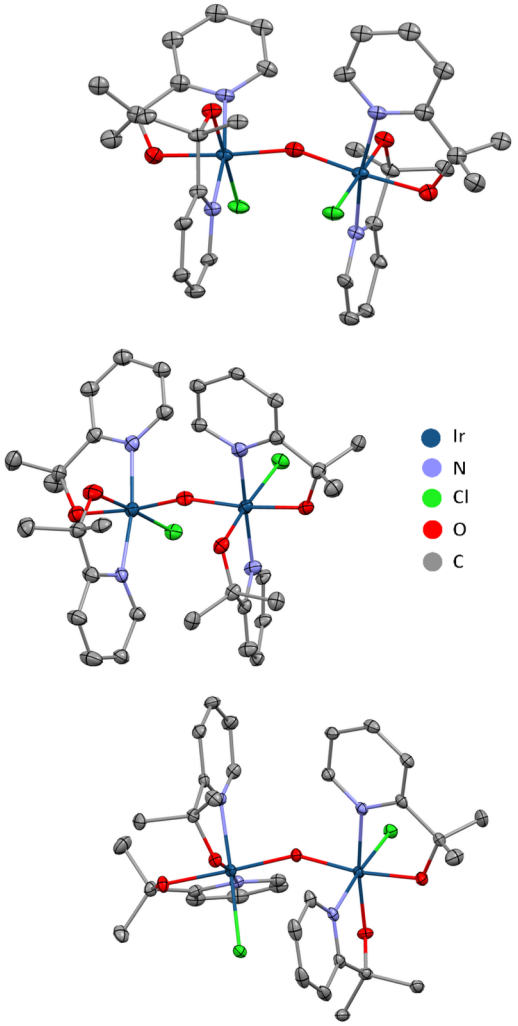

Figure 3. Thermal ellipsoid diagrams of the crystal structures of **gB1** (top), **gB2** (middle), and **rB1** (bottom) at 50% probability level. Hydrogen atoms have been omitted for clarity.

with Ir(IV) species in all cases.[13] Additionally, for all three compounds the two iridium centers are nearly identical in terms of bond lengths, which is evidence for a (IV,IV) rather than a mixed (III,V) oxidation state. The ligand isomer geometry around the iridium atom is retained: **gB1** and **gB2** have the same ligand arrangement as **G**, while **rB1** retains that of **R**. **gB1** crystallizes as a mixture of Δ–Δ and Λ–Λ enantiomers, with C_2 rotational symmetry between the two monomeric fragments of either enantiomer. In contrast, **gB2** and **rB1** are Δ–Λ isomers, with a mirror plane between the

Table 1. Comparison of Selected Crystallographic Bond Distances (Å) and Angles (deg) for gB1, gB2, and rB1

	gB1[a]	gB2[a]	rB1[a]
Ir–O (alkoxo)	1.944(16)	1.950(19)	1.985(3)
Ir–O (oxo)	1.917(5)	1.905(17)	1.906(3)
Ir–N	2.04(2)	2.04(2)	2.048(3)
Ir–Cl	2.365(6)	2.378(6)	2.342(1)
∠Ir–O–Ir	156.4(13)	159.3(10)[b]	148.32(16)

[a]Bond lengths calculated as the average of all relevant distances in the asymmetric unit. [b]Bond angle calculated as average over the two molecules in the asymmetric unit.

monomeric fragments in the *syn* conformation. The Ir–O–Ir bond angles in **gB1**, **gB2**, and **rB1** are 156°, 159°, and 148°, respectively. The weakly bent oxo bridge in the (IV,IV) oxidation state points to a mono-μ-oxo being preferred over a di-μ-oxo in these complexes, since a di-μ-oxo core has Ir–O–Ir bond angles of around 110°. If so, the "blue solution" may be composed of mono-μ-oxo and not di-μ-oxo species, as recently suggested.[10] However, the Ir–O–Ir angle in **gB1** and **rB1** may be restricted by steric effects, as close contacts between ligands on each Ir atom suggest that further bending may not be possible.

To probe the oxidation states of the Ir centers, X-ray photoelectron spectroscopy (XPS) analysis was performed on **gB1** (Figure S9) and **rB1** (Figure S10). The results are consistent with the presence of C, O, N, Cl, and Ir in both samples (see Figure S8). The Ir 4f region for **gB1**, with peaks at 62.0 and 65.0 eV, corresponds closely to that of the Ir "blue solution" (62.4 and 65.3 eV) and is consistent with Ir(IV).[10,19] Similarly, **rB1** (Figure S10) has peaks in the Ir 4f region (62.6 and 65.5 eV) which are consistent with a Ir(IV) species. By comparison, Lin et al. have reported binding energies of 60.3 and 63.8 eV for a related Ir(III) complex.[20]

UV–visible spectra of **rB1**, **gB1**, and **gB2** (Figure 4) exhibit intense visible absorption bands with molar absorptivity up to 7000 $M^{-1}cm^{-1}$. The absorption bands around 600–700 nm, present in all three spectra, are similar to the ∼600 nm feature observed in the iridium "blue solution". A Raman spectrum of **gB1** was also obtained (Figure S13).

All three complexes give sharp ^{1}H NMR spectra with all peaks being assignable (Figures S1–S3). Compound **gB1** gives a set of peaks corresponding to two distinct pyalk ligands, consistent with its C_2 rotation axis. Compound **gB2**, on the other hand, shows broad ^{1}H NMR resonances at room temperature that de-coalesce on cooling to give sharp peaks assignable to four distinct pyalk ligands. Because **gB2** is a Δ–Λ isomer, the two halves of the dimer are equivalent by symmetry only at two specific rotational conformations about the Ir–O bonds (whereas a rotation axis always connects the monomeric fragments of **gB1**). While unhindered rapid rotation would cause the two halves to give equivalent signals, the structures of all three species suggest considerable steric hindrance to such rotation, with pyridyl and methyl groups from both halves interlocking across the equatorial plane. The variable temperature ^{1}H NMR data are consistent with the eventual freezing of rotation and convergence to a single rotamer at low temperature; this is most likely the orientation displayed in the crystal structure, but even if not, it is expected to be different from the two symmetric positions as both are eclipsed conformations. At higher temperatures, rotation is faster, approaching a regime where both halves of the molecule

DOI: 10.1021/jacs.6b07716
J. Am. Chem. Soc. 2016, 138, 15917–15926

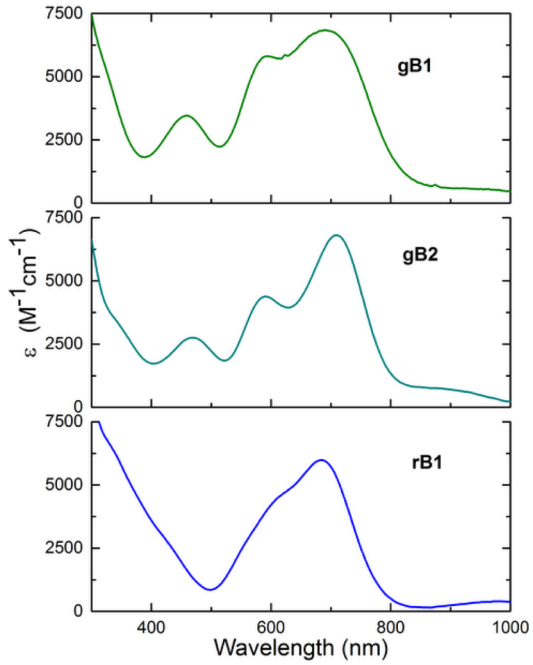

Figure 4. UV−visible absorption spectra for **gB1** (top), **gB2** (middle), and **rB1** (bottom) in dichloromethane.

experience equivalent average environments. Lineshape analysis of the VT NMR data for **gB2** (Figure S12) give a rotation barrier of $\Delta G^{\ddagger}$ = 11.5 kcal/mol. Surprisingly, **rB1**, which is also a Δ−Λ isomer, does not show line broadening effects between room temperature and −80 °C. This suggests fast rotation even at low temperatures.

While the ^{1}H NMR resonances are sharp for **gB1**, **rB1**, and **gB2** in the low-temperature regime, the peak positions are somewhat displaced from what is expected. For example, for **gB1**, aliphatic peaks range from −0.9 to 6.6 ppm, while aromatic peaks range from 5.1 to 10.4 ppm (Figure S1). These NMR shifts could be attributed to ring current effects,[21] paramagnetism due to a low-lying triplet state, or a combination of the two. SQUID magnetic susceptibility and EPR measurements suggest that the complex is diamagnetic: **gB1** does not show detectable paramagnetic behavior in SQUID measurements between 3 and 300 K, and in addition, it is EPR silent, consistent with diamagnetism as in the "blue solution". However, very weak paramagnetism from slight occupation of a triplet state cannot be ruled out. Previous studies have explored the electronic structures of other mono-μ-oxo Ir and Ru dimers isoelectronic with **gB1**.[15a,18] The previous Ir(IV,IV) dimers showed diamagnetic ^{1}H NMR spectra, and multi-configurational calculations assigned an antiferromagnetically coupled ground state and a much higher, unpopulated triplet state.[15a] In contrast, previous Ru(III,III) dimers are paramagnetic based on NMR and SQUID measurements and have a singlet ground state with a low-lying triplet.[18,22] In the Ru system, there has been debate over the degree of antiferromagnetic coupling in the ground state, underscoring the potential difficulty of determining the electronic state in these systems.[18,23]

Computational Studies. The electronic structure of **gB1** was further explored using DFT calculations. The crystal structure of the Ir(IV)−O−Ir(IV) dimer was fully optimized at the DFT(PBE)/LANL2TZ(f),6-311G** level considering the full real complex in a closed shell singlet state (**CSS**). The differences between the experimental and computational geometric parameters are small, with a root-mean-square

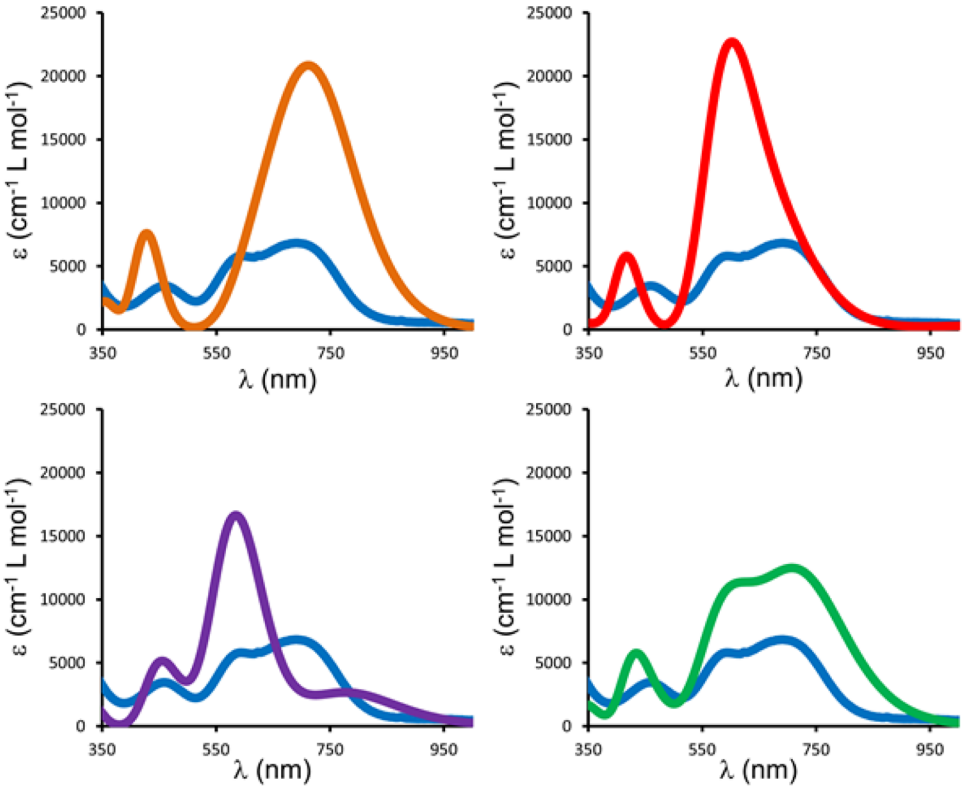

Figure 5. TD-DFT **CSS** (orange), **T** (red), **OSS** (purple), **CSS:OSS** 1.19:1.00 (green) vs experimental (blue) UV−visible spectra of **gB1**.

DOI: 10.1021/jacs.6b07716
J. Am. Chem. Soc. 2016, 138, 15917−15926

deviation (RMSD) for the Ir−O, Ir−N, and Ir−Cl distances of 0.034 Å. The PBE functional was selected based on its superior performance compared with other pure and hybrid DFT functionals, which yield similar or slightly larger RMSDs (Table S4). The experimental Ir−O−Ir bond angle, α = 156.2°, is also well reproduced by the calculations, α = 150.6°. This structural feature facilitates the in-phase combinations of the iridium d orbitals with the μ-O s and p orbitals.[15a] The triplet state was also fully optimized at the same level of theory and yields an energy minimum (**T**), although its geometry deviates more from the crystal structure (Figure S17), RMSD = 0.038 Å, and has a linear rather than angular Ir−O−Ir bridge, α = 177.7°. Despite these larger deviations, which were also obtained by all other functionals (Table S4), **T** was computed to be only 0.1 kcal mol^{-1} less stable than the **CSS**. Nonetheless, crystal-packing effects, not included in the DFT model, may stabilize the **CSS** state via weak, non-covalent interactions. A recent study on a similar system also suggests that the **CSS** state may be stabilized over **T** due to non-dynamical correlation effects.[15a] The greater stability of the **CSS** state is in agreement with the diamagnetic behavior of **gB1** observed experimentally by SQUID measurements (see above).

The UV−visible spectrum of **gB1** was calculated using both the **CSS** and **T** structures (see below); however, each state showed substantial deviations from the experimental UV−visible spectrum. One potential explanation for this result is the presence of another electronic state of similar energy to the **CSS**. To explore this possibility, we studied the open-shell singlet state (**OSS**). The optimized **OSS** geometry, studied at the same level of theory as the **CSS**, is very similar to that of **CSS** (Table S4 and Figure S17), having an identical RMSD from the X-ray structure, 0.034 Å, and a very similar Ir−O−Ir bond angle, α = 151.3°. The **OSS** is an antiferromagnetic state with the α and β spin densities spatially separated and located over the two metal centers (and to a lesser extent the alkoxo atoms), as shown by the opposite sign of their local spin densities: + and −0.29 a.u. (Figures S17 and S18). This spin state is calculated to be 0.3 kcal mol^{-1} more stable than **CSS**. However, whereas the apparent disagreement between the experimental and computational structures of **T** allows us to exclude this state, the small differences between the structures and energies of **CSS** and **OSS** leave both as possibilities for the ground state of the system.

The UV−visble spectrum of the Ir(IV)−O−Ir(IV) dimer was simulated by means of single-point TD-DFT(ωB97xd)/LANL2TZ(f),6-311G** calculations including solvation by dichloromethane with the continuum SCRF-SMD model, which was also used to re-optimize the geometries at the DFT(PBE)/LANL2TZ(f),6-311G** level. Figures 5 and 6 show the experimental and computational spectra overlapped. For the **CSS** state, the TD-DFT spectrum has two absorbance peaks, with λ_{max} at 709.2 nm, which deviates from the experimental value by 17.2 nm. The calculations do not reproduce the shoulder of the main band at 585 nm and yield a higher deviation of 33.5 nm for the near-UV secondary peak. The TD-DFT spectrum of the **T** state yielded higher deviations of 44.2 and 89.6 nm for the near-UV and near-IR bands, respectively. Interestingly, the two absorbance bands predicted for the **OSS** state deviate by only ca. 5 nm for both the near-UV peak and the shoulder of the near-IR peak. In line with these data, the best agreement with the experiments was reached by adding the **CSS** and **OSS** TD-DFT spectra in a 1.19:1.00 ratio, respectively, derived from the Gibbs energy difference between

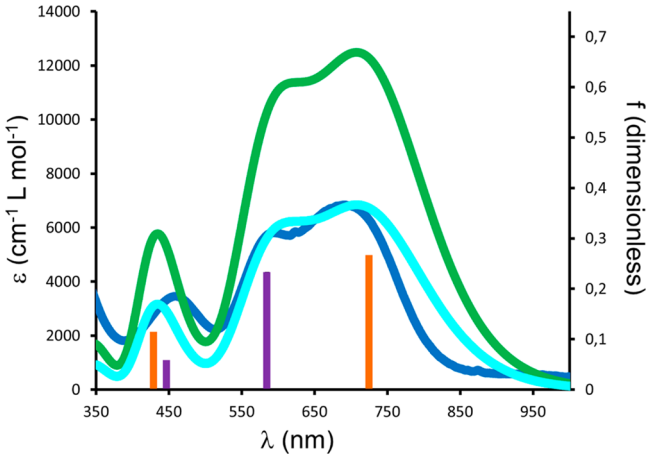

Figure 6. TD-DFT **CSS:OSS** 1.19:1.00 (normalized and non-normalized in light and dark green, respectively) vs experimental (blue) UV−visible spectra with sharp lines showing the main electronic transitions in the **CSS** (orange) and **OSS** (purple) states.

these two spin states in dichloromethane, 0.1 kcal mol^{-1}. These results suggest that the experimental UV−visible spectrum of the dimer complex may result from a mixture of two different electronic configurations in a multireference ground state. This would be consistent with the equal spin multiplicity, similar energy, and close electronic and geometric structures of **CSS** and **OSS**. The multireference nature of **gB1** is currently being further investigated by means of DMRG-CASSCF calculations.

Unfortunately, no conclusive experimental data could be obtained to support the above assignment, and the issue of coupling has not been decisively resolved for the more extensively studied Ru systems either,[18,23] leaving room for other interpretations. One possibility is that torsion about the oxo bridge perturbs the frontier electronic structure; indeed, we see extensive π-delocalization across the bridging oxo (Figure 7), which would be expected to be rotation-sensitive. The NMR data presented earlier are consistent with rotation being sufficiently unhindered to proceed at room temperature. While

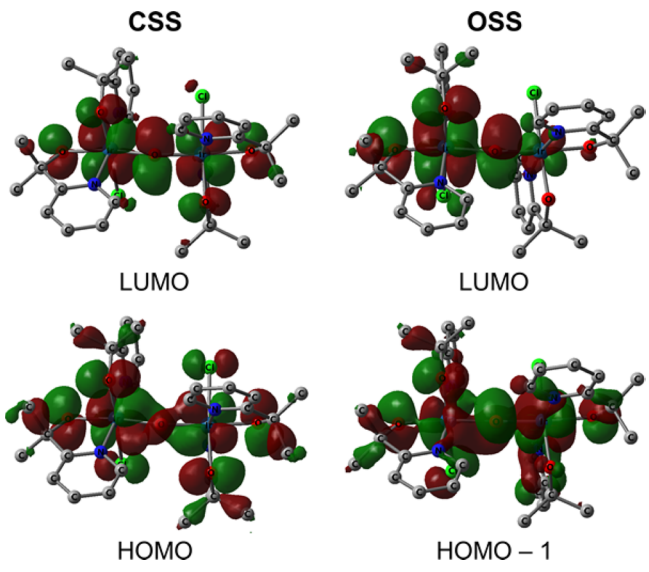

Figure 7. Principal molecular orbitals of **gB1** involved in the 550−750 nm absorptions for **CSS** (HOMO and LUMO) and **OSS** (HOMO−1 and LUMO).

DOI: 10.1021/jacs.6b07716
J. Am. Chem. Soc. 2016, 138, 15917−15926

our calculations were for a single structure, the presence of a distribution of rotational conformers could give a range of spectra that combine to give the observed spectrum. Regardless, the extensive delocalization of the key frontier orbitals demonstrates the strong electronic coupling between the two metal centers.

The TD-DFT calculations for **gB1** were also used to determine the main electronic transitions responsible for the band with the highest intensity in the far-red region of the spectrum responsible for the blue color. The main contribution from the **CSS** state is the electronic transition at 725.5 nm with an oscillator strength (f) of 0.254. This transition involves the HOMO and LUMO orbitals of the system. The main contribution from the **OSS** state is the electronic transition at 584.7 nm with f = 0.229, involving the HOMO−1 and LUMO orbitals.

Because intense absorption features leading to a blue color seem to almost always accompany formation of Ir(IV) or Ru(III) oxo dimers,[16b,23] we looked at the relevant transitions in more detail. The three frontier orbitals involve nonbonding and antibonding combinations of the iridium d and oxygen p orbitals (Figure 7). The HOMO → LUMO (**CSS**) and HOMO−1 → LUMO (**OSS**) transitions can thus be both described as $n \rightarrow \pi^*$ excitations. It is evident from the MO structures that these transitions do not belong to the common types of excitation seen in coordination compounds: there are no signs of charge transfer between Ir and ligands, and the oscillator strength is far too high for simple d−d excitation. Instead, all participating orbitals are delocalized, primarily over the Ir−O−Ir core. We, therefore, categorize these transitions as excitations of a conjugated π-system involving Ir d and oxo p orbitals. This classification helps to explain the low energy excitation gap (far-red absorption), the high absorption intensity, and the insensitivity toward changes in the ligand environment. Whereas normal d−d transitions have weak absorptivity due to the Laporte rule, delocalized combinations of d orbitals on two separate centers can have either odd or even parity. Therefore, transitions between such orbitals can have much higher absorptivity. This is most distinctly exemplified by the **CSS** HOMO−LUMO transition. The Ir d orbitals in the HOMO couple to an overall even parity with respect to the center of the molecule, while the d orbitals in the LUMO, along with an oxo p orbital, result in odd parity with respect to the center of the molecule. The high orbital overlap, combined with the proper parity, results in a high molar absorptivity. The absorption near 430 nm, on the other hand, appears to be mostly a ligand-to-metal charge transfer (LMCT) from delocalized O, Cl p orbitals to the LUMO, with lesser involvement of metal-centered orbitals.

This leads to another observation: the LMCT bands, which typically dominate the visible region of Ir(IV) monomers,[13] are, aside from the above example, absent above 400 nm. The main reason for this appears to be that the frontier metal-centered orbitals are higher in energy relative to the ligand MOs, as evidenced by the fact that the 430 nm excitation involves the highest predominantly ligand-based MOs. This helps explain a puzzling observation: Ir(IV) monomers display wide-ranging visible spectra, leading to very varied colors, as is the case for our monomeric precursors. In contrast, Ir(IV) oxo dimers have a characteristic absorption pattern with peaks at 600 nm or higher, low absorption around 400−500 nm, and a sharp increase below 400 nm; this consistently gives them a blue or closely related color. Dimers seem to display very limited involvement of LMCT's in the visible region, allowing their visible spectra, and therefore color, to be dominated by the dimer transitions. Because those primarily involve the Ir−O−Ir core, their energies would not be expected to change greatly with variation of the auxiliary ligands. We observe this in comparisons between the spectra of **rB1** and **gB1**/**gB2** which vary minimally, mostly in respect of just one LMCT band. Their parent monomers, on the other hand, display entirely dissimilar spectra.[13]

Another interesting observation is that the crystals of **gB1** and **rB1** are light brown in color, despite the fact that the complexes are deep blue in solution. This initially led us to suspect they contained degradation products. However, numerous cycles of precipitation and dissolution, as well as NMR measurements, showed that the crystals did indeed contain only one pure compound. Based on the crystal and electronic structures, we attribute this phenomenon to the mutual alignment of the transition dipole moments of the visible transitions. In both crystal structures, the molecules are packed so that all the Ir−Ir axes are oriented in the same direction. Furthermore, the geometries of all relevant frontier orbitals are such that the transition dipoles of the red-light absorptions are all aligned along the Ir−Ir axis; excitation can therefore only be induced by radiation polarized along that axis. Because these are the main visible-light transitions of the compound, single crystals can only absorb visible light of one polarization, meaning that a large fraction of unpolarized light is transmitted regardless of the high molar absorptivity. Indeed, the crystals behave as polarizers: rotating them under a single polarizer results in alternating extinction and transmission. In contrast, the crystals of **gB2**, in which there are four distinct Ir−Ir orientations, are extremely dark blue in color, as would be expected from the solution-phase appearance. This observation emphasizes the potential importance of crystal packing in determining the visual appearance of crystals beyond what may be expected from an amorphous or dissolved state.

CONCLUSION

We have prepared, isolated, and characterized a series of iridium mono-μ-oxo dimers containing the pyalk ligand. They are the first examples of stable Ir(IV,IV) oxo dimer coordination complexes and serve as models for the "blue solution" WOC, which is proposed[10,11] to contain pyalk ligands and a mono-μ-oxo core. Whereas the "blue solution" contains many isomers that are not separable, the complexes studied here are prepared by coupling pure monomers, resulting in specific isomers. Importantly, we were able to separate these species by preparative TLC, allowing for characterization of single isomers, still impossible for the "blue solution". In contrast to the previously reported Ir-oxo dimers, the ones studied here are stable under ambient conditions. This facilitates their full characterization including by X-ray crystallography. The Ir-mono-μ-oxo core supported by pyalk ligands agrees with the recent computational study suggesting a similar structure for the "blue solution".[11] Ongoing work is focused on comparing the redox properties and catalytic activity of these and related isomers with the aim of identifying the structural features that promote WO catalysis.

EXPERIMENTAL AND COMPUTATIONAL METHODS

Physical Methods. *NMR Spectroscopy.* NMR spectra (^{1}H and ^{13}C {^{1}H}) were recorded on an Agilent DD2 600 MHz spectrometer

DOI: 10.1021/jacs.6b07716
J. Am. Chem. Soc. 2016, 138, 15917−15926

equipped with a chilled probe. Chemical shifts are reported after calibration with solvent residual peaks.

High-Resolution Mass Spectroscopy (HRMS). Mass spectrometry analyses were performed by the Mass Spectrometry and Proteomics Resource of the W.M. Keck Foundation Biotechnology Resource Laboratory at Yale University, using a 9.4 T Bruker Qe FT-ICR MS instrument in positive ion mode.

UV−Visible Spectroscopy. Absorption spectra were collected using a Cary 50 spectrophotometer for solutions of 0.1 mM in dichloromethane.

X-ray Photoelectron Spectroscopy (XPS) Spectroscopy. XPS (**gB1** and **rB1**) was performed on a Phi 5500 instrument using Al Kα photons ($h\nu$ = 1486.6 eV). The sample was prepared by drop-casting a concentrated solution of the compound on a Si substrate (1 cm^2) coated with a thin Au film. The sample was evacuated for ∼5 h under high vacuum. The peaks were fitted using the XPST 1.1 extension on Igor Pro. This fitting program uses a Gauss−Lorentzian sum function to approximate a Voigt profile.

Raman Spectroscopy. Raman spectroscopy was performed on drop-cast samples of **gB1** and "blue solution" using a Horiba Labram HR Evolution instrument. Laser radiation of 633 nm was used for the data collection.

SQUID Magnetometry. The DC magnetic susceptibility of **gB1** was measured using a Cryogenic R-700X SQUID magnetometer. The powder sample (12 mg) was loaded into a gel capsule inside a nitrogen-filled glovebox and then mounted in a clear plastic straw. We measured the temperature dependence of the magnetization of the sample from 3 to 300 K in a 100 mT external field. The signal was diamagnetic and on the order of magnitude of the background. We then measured the field dependence of the magnetization of the sample at 100 K in the range 0 to 7 T.

Computational Details. Geometries were fully optimized without any geometry or symmetry constraint with different pure (BP86,[24] M06L,[25] TPSS,[26] and PBE[27]) and hybrid (B3LYP,[28] M06,[29] TPSSh,[26] and PBE0[30]) DFT functionals implemented in the Gaussian09 program, due to the influence of the amount of HF-exchange on the energy difference between low and high spin states.[31] The influence of the dispersion forces was also considered by using Grimme's GD3BJ model.[32] The pruned ultrafine (99,590) grid was used for a highly accurate calculation of the two-electron integrals. All elements except iridium were described with the all-electron polarized valence triple-ζ 6-311G** basis set.[33] Iridium was described with the LANL2TZ(f) basis set[34] including a Hay-Wadt relativistic effective core potential. Vibrational frequencies were computed analytically to confirm that all stationary points located in the potential energy hypersurface were minima. These calculations were also used to derive the thermochemistry, including the zero-point, thermal, and entropy energies. For the comparison to the experimental X-ray crystal structures, geometries were optimized in the gas phase. For the comparison to the experimental UV−visible spectra, geometries were optimized in dichloromethane solution with the continuum SCRF-SMD method.[35] The latter geometries were used to determine the wavelengths and intensities of the electronic transitions in the UV−visible spectra by means of single-point SCRF-SMD (dichloromethane) TD-DFT calculations with the hybrid ωB97xd functional,[36] which contains both dispersion and long-range corrections. The convolution of the computational data required to construct the TD-DFT spectra was done by fitting to Gaussian functions with a bandwidth at half-height of 3000.0 cm^{-1}, as implemented in the AOMix software.[37] The unrestricted approach was used in the optimization of the triplet and open-shell singlet states. In the latter case, molecular fragments with different charges and multiplicities were combined to obtain the broken-symmetry DFT solution. The energy of this state was corrected with the Yamaguchi approach to spin contamination.[38] The stability of all electronic states was verified after convergence by means of perturbative electronic excitations.

Synthesis. *General.* Reagents and solvents were purchased from commercial sources and used as received without further purification, except for dichloromethane (DCM) and dichloroethane (DCE), which were purified according to prior literature.[1] The ligand Hpyalk was prepared according to prior literature.[2] All other manipulations were carried out under ambient atmosphere. Pressurized high-temperature reactions were carried out in a Biotage Initiator microwave synthesizer.

*Optimized Preparation of mer- and fac-Tris(2-{pyridin-2-yl}-propan-2-olato)iridium(III) (**Ir(pyalk)$_3$**).* To a 20 mL Biotage microwave vial were added 708 mg of $IrCl_3 \cdot 3H_2O$ (2 mmol), 1.64 g of Hpyalk (12 mmol), and 20 mL of water. The vial was sealed and heated under microwave irradiation (120 °C, 45 min). After cooling to room temperature, the solution was basified with a saturated solution of $NaHCO_3$. The aqueous phase was extracted several times with DCM until the aqueous layer appeared light yellow in color and the organic layer was mostly colorless. The organic extract was reduced in volume by evaporation under reduced pressure to a dark red-brown viscous residue. To remove excess free ligand, the residue was diluted with approximately 5 mL of DCM and then partially precipitated with 30 mL of *n*-octane. The mixture was heated along with manual stirring/grinding to the boiling point of *n*-octane, while DCM was allowed to evaporate. The viscous precipitate gradually solidified while being ground to a powder. The mixture was cooled, the solvent decanted, and the process repeated once more. The resulting brick orange powder was dried under reduced pressure. Yield: **Ir(pyalk)$_3$** (1.17 g, 1.8 mmol, 90%). The effective molar mass for the Ir(pyalk)$_3$ complexes was taken to be ∼650 g/mol due to solvent and counterion contributions (contains a mixture of Ir(III) and Ir(IV) states).

*Preparation and Isolation of cis-Cl,cis-O,trans-N-Bis(2-{pyridin-2-yl}propan-2-olato)dichloroiridium(IV)] (Green Isomer, **G**) and cis-Cl,cis-O,cis-N-Bis(2-{pyridin-2-yl}propan-2-olato)dichloroiridium(IV) (Red Isomer, **R**).* To a Biotage microwave vial (size 20 mL) were added 840 mg of **Ir(pyalk)$_3$** (1.3 mmol) and 20 mL of 1 M aq. HCl/acetone (1:4). The vial was sealed and heated under microwave irradiation (140 °C, 45 min). After cooling to room temperature, the solvent was reduced by evaporation under reduced pressure. The mixture was then diluted with 20 mL of water, and excess sodium periodate was added, giving rapid oxidation to Ir(IV) species and a color change from yellow to dark red. [***Caution**: Some Cl_2 is produced during this step, but remains largely in solution.*] The solution was extracted with 4 × 20 mL portions of DCM, until the aqueous layer was pale in color. The organic layer was dried with $MgSO_4$, filtered, and evaporated to dryness.

The green and red isomers were separated from the crude mixture by silica column chromatography. First, elution with a 0.5:0.35:0.15 acetone/hexanes/EtOAc solution gave pure **R** and separated **G** from most of the other isomers. A second column with 3:1 DCM/EtOAc gave the green isomer as a pure species. Yield: **G** (70 mg, 0.13 mmol, 10%), **R** (417 mg, 0.78 mmol, 60%)

*Preparation of **gB1** and **gB2**.* To a 2 mL solution of DCE (predried using $MgSO_4$) were added 150 mg of **G** (0.28 mmol) and 1.5 g of $MgSO_4$. One gram of Ag_2O was added to the vial, and the mixture was heated at reflux for 15−20 min, giving a color change from green to deep blue. Small amounts of Ag_2O were added to the reaction mixture at regular intervals for the duration of the reaction. The reaction was followed by TLC and stopped once all of **G** was consumed.

The crude mixture from the Ag_2O reaction was cooled and filtered through a fine frit, and the solid was extracted multiple times with DCM and finally acetone. The filtrate was evaporated to dryness, redissolved in 1 mL of DCM, and loaded on a preparative TLC plate. The plate was run in a mixture of 8% water in acetone. The two major blue bands, containing **gB1** (first band) and **gB2** (second band), were collected by scraping the silica gel, crushing into a fine powder, and eluting through a frit with an acetone/water mixture (up to 50% water). The filtrates were dried *in vacuo*, redissolved in DCM, and filtered to remove any remaining silica. The residues were further purified by precipitation from a saturated DCM solution with pentane followed by filtration and further washing with pentane. Crystals of **gB1** were grown as thin brown plates by layering a DCM solution of **gB1** with octane and storing at −20 °C for several days in a slightly open container to facilitate the slow evaporation of DCM. Crystals of

DOI: 10.1021/jacs.6b07716
J. Am. Chem. Soc. 2016, 138, 15917−15926

gB2 were grown as dark blue needles from a layered DCM/pentane solution at −20 °C.

Yield **gB1** (32.5 mg, 22%); ^{1}H NMR (600 MHz, methylene chloride-d_2) δ 10.39−10.34 (m, 2H), 8.72 (d, J = 5.4 Hz, 2H), 8.52−8.41 (m, 4H), 7.92−7.86 (m, 2H), 7.33−7.25 (m, 2H), 7.00 (dd, J = 5.6, 1.4 Hz, 2H), 6.56 (s, 6H), 5.14 (dd, J = 8.2, 1.4 Hz, 2H), 3.94 (s, 6H), 2.51 (s, 6H), −0.86 (s, 6H). ^{13}C NMR (151 MHz, methylene chloride-d_2) δ 177.75 (ar), 168.13 (ar), 142.65 (ar), 141.98 (ar), 141.91 (ar), 138.23 (ar), 121.39 (ar), 121.34 (ar), 119.58 (ar), 116.65 (ar), 81.82, 79.00, 76.77, 74.94, 63.81, 29.66. HRMS (FT-ICR): calcd for [$C_{32}H_{40}Cl_2Ir_2N_4O_5$]: 1017.1693 ($z$ = 1+), found m/z = 1017.1703 (z = 1+).

Yield: **gB2** (10 mg, 7%); ^{1}H NMR (500 MHz, methylene chloride-d_2, T = −70 °C) δ 9.45 (s, 1H), 8.41 (d, J = 6.8 Hz, 1H), 8.19 (s, 1H), 8.02 (d, J = 9.1 Hz, 2H), 7.72 (t, J = 7.9 Hz, 1H), 7.68−7.58 (m, 2H), 7.58−7.42 (m, 3H), 6.87 (d, J = 7.9 Hz, 1H), 6.82 (d, J = 8.1 Hz, 1H), 6.73−6.61 (m, 3H), 3.19 (s, 3H), 2.36 (s, 3H), 2.25 (s, 6H), 1.72 (s, 3H), 1.52 (s, 3H), 1.19 (s, 4H), 1.01 (s, 3H), 0.71 (s, 3H). HRMS (FT-ICR): calcd for [$C_{32}H_{40}Cl_2Ir_2N_4O_5$]: 1017.1693 ($z$ = 1+), found m/z = 1017.1721 (z = 1+).

Preparation of ***rB1***. To a 2 mL solution of DCE (predried using $MgSO_4$) were added 150 mg of **R** (0.28 mmol) and 1.5 g of $MgSO_4$. One gram of Ag_2O was added to the vial, and the mixture was heated at reflux for 2−5 min, giving a color change from red to dark green. The same separation technique was followed as for the green isomer, yielding **rB1** by collecting the top major blue band from the preparative TLC. Crystals of **rB1** were grown as thin yellow plates from a layered DCM/pentane solution at −20 °C.

Yield **rB1** (13 mg, 9%); ^{1}H NMR (500 MHz, methylene chloride-d_2) δ 11.20 (t, J = 6.7 Hz, 2H), 9.80 (d, J = 5.5 Hz, 2H), 8.03 (t, J = 6.6 Hz, 2H), 7.97 (td, J = 7.9, 1.5 Hz, 2H), 7.87 (d, J = 7.8 Hz, 2H), 7.51 (td, J = 7.6, 1.4 Hz, 2H), 7.40 (d, J = 5.6 Hz, 2H), 6.42 (d, J = 8.0 Hz, 2H), 3.59 (s, 6H), 1.34 (s, 6H), 0.50 (s, 6H), −0.65 (s, 6H). ^{13}C NMR (151 MHz, methylene chloride-d_2) δ 175.72 (ar), 155.10 (ar), 146.37 (ar), 143.39 (ar), 138.61 (ar), 128.82 (ar), 120.82 (ar), 118.61(ar), 117.80 (ar), 116.68 (ar), 97.72, 82.82, 65.34, 61.91, 60.44, 46.41. HRMS (FT-ICR): calcd for [$C_{32}H_{40}Cl_2Ir_2N_4O_5$]: 1017. 1693 ($z$ = 1+), found m/z = 1017.1667 (z = 1+).

■ ASSOCIATED CONTENT

Supporting Information

The Supporting Information is available free of charge on the ACS Publications website at DOI: 10.1021/jacs.6b07716.

Additional ^{1}H and ^{13}C NMR spectra, HRMS and XPS data, Raman spectra and computational details, crystallographic details and procedures, DFT-optimized geometries and energies, and additional Figures S1−S18 (PDF)

Crystal structure file for **gB1** (CIF)

Crystal structure file for **gB2** (CIF)

Crystal structure file for **rB1** (CIF)

■ AUTHOR INFORMATION

Corresponding Authors

*david.balcells@kjemi.uio.no

*gary.brudvig@yale.edu

*robert.crabtree@yale.edu

ORCID

Liam S. Sharninghausen: 0000-0002-2249-1010

Shashi Bhushan Sinha: 0000-0002-3212-7570

David Balcells: 0000-0002-3389-0543

Author Contributions

‡L.S.S., S.B.S., and D.Y.S. contributed equally.

Notes

The authors declare no competing financial interest.

■ ACKNOWLEDGMENTS

This work (L.S.S, S.B.S., and D.Y.S) was supported the U.S. Department of Energy, Office of Science, Office of Basic Energy Sciences, Division of Chemical Sciences, Geosciences, and Biosciences under Award Number DE-SC0001059 as part of the Argonne-Northwestern Solar Energy Research (ANSER) Energy Frontier Research Center (spectroscopy and characterization) and under Award Number DEFG02-07ER15909 (synthesis). B.C. is supported by the NSF Graduate Research Fellowship under Grant No. DGE 11-44155. D.B. thanks the Research Council of Norway for funding provided through the Centre of Excellence for Theoretical and Computational Chemistry (CTCC; Grant 179568/V30), the Norwegian Metacenter for Computational Science (NOTUR; Grant nn4654k), the EU REA for a Marie Curie Fellowship (Grant CompuWOC/618303), and Odile Eisenstein for fruitful discussions. Dr. Min Li and Zishan Wu (Yale) are acknowledged for access to XPS and Raman spectroscopy.

■ REFERENCES

(1) (a) Lewis, N. S.; Nocera, D. G. *Proc. Natl. Acad. Sci. U. S. A.* **2006**, *103*, 15729. (b) Blankenship, R. E.; Tiede, D. M.; Barber, J.; Brudvig, G. W.; Fleming, G.; Ghirardi, M.; Gunner, M. R.; Junge, W.; Kramer, D. M.; Melis, A.; Moore, T. A.; Moser, C. C.; Nocera, D. G.; Nozik, A. J.; Ort, D. R.; Parson, W. W.; Prince, R. C.; Sayre, R. T. *Science* **2011**, *332*, 805. (c) Meyer, T. J. *Acc. Chem. Res.* **1989**, *22*, 163. (d) Alstrum-Acevedo, J. H.; Brennaman, M. K.; Meyer, T. J. *Inorg. Chem.* **2005**, *44*, 6802. (e) Gust, D.; Moore, T. A.; Moore, A. L. *Acc. Chem. Res.* **2009**, *42*, 1890. (f) Karkas, M. D.; Verho, O.; Johnston, E. V.; Åkermark, B. *Chem. Rev.* **2014**, *114*, 11863. (g) Blakemore, J. D.; Crabtree, R. H.; Brudvig, G. W. *Chem. Rev.* **2015**, *115*, 12974. (h) Parent, A. R.; Sakai, K. *ChemSusChem* **2014**, *7*, 2070.

(2) (a) Dau, H.; Limberg, C.; Reier, T.; Risch, M.; Roggan, S.; Strasser, P. *ChemCatChem* **2010**, *2*, 724. (b) Meekins, B. H.; Kamat, P. V. *J. Phys. Chem. Lett.* **2011**, *2* (18), 2304. (c) Parent, A. R.; Nakazono, T.; Lin, S.; Utsunomiya, S.; Sakai, K. *Dalton Trans.* **2014**, *43*, 12501. (d) Pokhrel, R.; Goetz, M. K.; Shaner, S. E.; Wu, X.; Stahl, S. S. *J. Am. Chem. Soc.* **2015**, *137*, 8384. (e) Wasylenko, D. W.; Palmer, R. D.; Berlinguette, C. P. *Chem. Commun.* **2013**, *49*, 218.

(3) (a) Rohde, J. U.; Lee, W. T. *J. Am. Chem. Soc.* **2009**, *131*, 9162. (b) Blakemore, J. D.; Mara, M. W.; Kushner-Lenhoff, M. N.; Schley, N. D.; Konezny, S. J.; Rivalta, I.; Negre, C. F. A.; Snoeberger, R. C.; Kokhan, O.; Huang, J.; Stickrath, A.; Tran, L. A.; Parr, M. L.; Chen, L. X.; Tiede, D. M.; Batista, V. S.; Crabtree, R. H.; Brudvig, G. W. *Inorg. Chem.* **2013**, *52*, 1860. (c) Blakemore, J. D.; Schley, N. D.; Kushner-Lenhoff, M. N.; Winter, A. M.; D'Souza, F.; Crabtree, R. H.; Brudvig, G. W. *Inorg. Chem.* **2012**, *51*, 7749.

(4) Hull, J. F.; Balcells, D.; Blakemore, J. D.; Incarvito, C. D.; Eisenstein, O.; Brudvig, G. W.; Crabtree, R. H. *J. Am. Chem. Soc.* **2009**, *131*, 8730.

(5) (a) Blakemore, J. D.; Schley, N. D.; Balcells, D.; Hull, J. F.; Olack, G. W.; Incarvito, C. D.; Eisenstein, O.; Brudvig, G. W.; Crabtree, R. H. *J. Am. Chem. Soc.* **2010**, *132*, 16017. (b) Schley, N. D.; Blakemore, J. D.; Subbaiyan, N. K.; Incarvito, C. D.; D'Souza, F.; Crabtree, R. H.; Brudvig, G. W. *J. Am. Chem. Soc.* **2011**, *133*, 10473. (c) DePasquale, J.; Nieto, I.; Reuther, L. E.; Herbst-Gervasoni, C. J.; Paul, J. J.; Mochalin, V.; Zeller, M.; Thomas, C. M.; Addison, A. W.; Papish, E. T. *Inorg. Chem.* **2013**, *52*, 9175. (d) Hetterscheid, D. G. H.; Reek, J. N. H. *Chem. Commun.* **2011**, *47*, 2712. (e) Hong, D.; Murakami, M.; Yamada, Y.; Fukuzumi, S. *Energy Environ. Sci.* **2012**, *5*, 5708. (f) Lalrempuia, R.; McDaniel, N. D.; Müller-Bunz, H.; Bernhard, S.; Albrecht, M. *Angew. Chem., Int. Ed.* **2010**, *49*, 9765. (g) Lewandowska-Andralojc, A.; Polyansky, D. E.; Wang, C.-H.; Wang, W.-H.; Himeda, Y.; Fujita, E. *Phys. Chem. Chem. Phys.* **2014**, *16*, 11976. (h) Thomsen, J. M.; Huang, D. L.; Crabtree, R. H.; Brudvig, G. W. *Dalton Trans.* **2015**, *44*, 12452.

DOI: 10.1021/jacs.6b07716
J. Am. Chem. Soc. 2016, 138, 15917−15926

(6) (a) Park-Gehrke, L. S.; Freudenthal, J.; Kaminsky, W.; DiPasquale, A. G.; Mayer, J. M. *J. Chem. Soc., Dalton Trans.* **2009**, *11*, 1972. (b) Zuccaccia, C.; Bellachioma, G.; Bortolini, O.; Bucci, A.; Savini, A.; Macchioni, A. *Chem. - Eur. J.* **2014**, *20*, 3446. (c) Savini, A.; Belanzoni, P.; Bellachioma, G.; Zuccaccia, C.; Zuccaccia, D.; Macchioni, A. *Green Chem.* **2011**, *13*, 3360. (d) Zuccaccia, C.; Bellachioma, G.; Bolaño, S.; Rocchigiani, L.; Savini, A.; Macchioni, A. *Eur. J. Inorg. Chem.* **2012**, *9*, 1462. (e) Liao, R. Z.; Siegbahn, P. E. M. *ACS Catal.* **2014**, *4*, 3937.
(7) Hintermair, U.; Hashmi, S. M.; Elimelech, M.; Crabtree, R. H. *J. Am. Chem. Soc.* **2012**, *134*, 9785.
(8) (a) Parent, A. R.; Brewster, T. P.; De Wolf, W.; Crabtree, R. H.; Brudvig, G. W. *Inorg. Chem.* **2012**, *51*, 6147−6152. (b) Thomsen, J. M.; Sheehan, S. W.; Hashmi, S. M.; Campos, J.; Hintermair, U.; Crabtree, R. H.; Brudvig, G. W. *J. Am. Chem. Soc.* **2014**, *136*, 13826.
(9) (a) Shopov, D. Y.; Rudshteyn, B.; Campos, J.; Batista, V. S.; Crabtree, R. H.; Brudvig, G. W. *J. Am. Chem. Soc.* **2015**, *137*, 7243. (b) Sinha, S. B.; Shopov, D. Y.; Sharninghausen, L. S.; Vinyard, D. J.; Mercado, B. Q.; Brudvig, G. W.; Crabtree, R. H. *J. Am. Chem. Soc.* **2015**, *137*, 15692.
(10) Hintermair, U.; Sheehan, S. W.; Parent, A. R.; Ess, D. H.; Richens, D. T.; Vaccaro, P. H.; Brudvig, G. W.; Crabtree, R. H. *J. Am. Chem. Soc.* **2013**, *135*, 10837.
(11) Yang, K. R.; Matula, A. J.; Kwon, G.; Hong, J.; Sheehan, S. W.; Thomsen, J. M.; Brudvig, G. W.; Crabtree, R. H.; Tiede, D. M.; Chen, L. X.; Batista, V. S. *J. Am. Chem. Soc.* **2016**, *138*, 5511.
(12) Huang, D. L.; Beltrán-Suito, R.; Thomsen, J. M.; Hashmi, S. M.; Materna, K. L.; Sheehan, S. W.; Mercado, B. Q.; Brudvig, G. W.; Crabtree, R. H. *Inorg. Chem.* **2016**, *55*, 2427.
(13) Shopov, D. Y.; Rudshteyn, B.; Campos, J.; Batista, V. S.; Crabtree, R. H.; Brudvig, G. W. *Chem. Sci.* **2017**, DOI: 10.1039/c6sc03758e.
(14) Sheehan, S. W.; Thomsen, J. M.; Hintermair, U.; Crabtree, R. H.; Brudvig, G. W.; Schmuttenmaer, C. A. *Nat. Commun.* **2015**, *6*, 6469.
(15) (a) Lehman, M. C.; Pahls, D. R.; Meredith, J. M.; Sommer, R. D.; Heinekey, D. M.; Cundari, T. R.; Ison, E. A. *J. Am. Chem. Soc.* **2015**, *137*, 3574. (b) Fortner, K. C.; Laitar, D. S.; Muldoon, J.; Pu, L.; Braun- Sand, S. B.; Wiest, O.; Brown, S. N. *J. Am. Chem. Soc.* **2007**, *129*, 588.
(16) (a) Castillo-Blum, S. E.; Richens, D. T.; Sykes, A. G. *J. Chem. Soc., Chem. Commun.* **1986**, *14*, 1120. (b) Castillo-Blum, S. E.; Richens, D. T.; Sykes, A. G. *Inorg. Chem.* **1989**, *28*, 954. (c) Bardin, M. B.; Ketrush, P. M. *Russ. J. Inorg. Chem. (Engl. Transl.)* **1973**, *18*, 693.
(17) Greenwood, N. N.; Earnshaw, A. *Chemistry of the Elements*; Elsevier: London, 1997; p 1118.
(18) Liu, F.; Concepcion, J. J.; Jurss, J. W.; Cardolaccia, T.; Templeton, J. L.; Meyer, T. J. *Inorg. Chem.* **2008**, *47*, 1727.
(19) Leigh, G. J.; Bremser, W. *J. Chem. Soc., Dalton Trans.* **1972**, 1216.
(20) Wang, C.; Wang, J.; Lin, W. *J. Am. Chem. Soc.* **2012**, *134*, 19895.
(21) Wannere, C. S.; Schleyer, P. V. R. *Org. Lett.* **2003**, *5*, 605.
(22) Weaver, T. R.; Meyer, T. J.; Adeyemi, S. A.; Brown, G. M.; Eckberg, R. P.; Hatfield, W. E.; Johnson, E. C.; Murray, R. W.; Untereker, D. *J. Am. Chem. Soc.* **1975**, *97*, 3039.
(23) Batista, E. R.; Martin, R. L. *J. Am. Chem. Soc.* **2007**, *129*, 7224.
(24) (a) Becke, A. D. *Phys. Rev. A: At., Mol., Opt. Phys.* **1988**, *38*, 3098. (b) Perdew, J. P. *Phys. Rev. B: Condens. Matter Mater. Phys.* **1986**, *33*, 8822.
(25) Zhao, Y.; Truhlar, D. G. *J. Chem. Phys.* **2006**, *125*, 194101.
(26) Tao, J. M.; Perdew, J. P.; Staroverov, V. N.; Scuseria, G. E. *Phys. Rev. Lett.* **2003**, *91*, 146401.
(27) (a) Perdew, J. P.; Burke, K.; Ernzerhof, M. *Phys. Rev. Lett.* **1996**, *77*, 3865. (b) Perdew, J. P.; Burke, K.; Ernzerhof, M. *Phys. Rev. Lett.* **1997**, *78*, 1396.
(28) Becke, A. D. *J. Chem. Phys.* **1993**, *98*, 5648.
(29) Zhao, Y.; Truhlar, D. G. *Theor. Chem. Acc.* **2008**, *120*, 215.
(30) Adamo, C.; Barone, V. *J. Chem. Phys.* **1999**, *110*, 6158.
(31) (a) Qayyum, M. F.; Sarangi, R.; Fujisawa, K.; Stack, T. D. P.; Karlin, K. D.; Hodgson, K. O.; Hedman, B.; Solomon, E. I. *J. Am. Chem. Soc.* **2013**, *135*, 17417. (b) Cirera, J.; Paesani, F. *Inorg. Chem.* **2012**, *51*, 8194.
(32) Grimme, S.; Ehrlich, S.; Goerigk, L. *J. Comput. Chem.* **2011**, *32*, 1456.
(33) Krishnan, R.; Binkley, J. S.; Seeger, R.; Pople, J. A. *J. Chem. Phys.* **1980**, *72*, 650.
(34) (a) Hay, P. J.; Wadt, W. R. *J. Chem. Phys.* **1985**, *82*, 299. (b) Roy, L. E.; Hay, P. J.; Martin, R. L. *J. Chem. Theory Comput.* **2008**, *4*, 1029.
(35) Marenich, A. V.; Cramer, C. J.; Truhlar, D. G. *J. Phys. Chem. B* **2009**, *113*, 6378.
(36) Chai, J. D.; Head-Gordon, M. *Phys. Chem. Chem. Phys.* **2008**, *10*, 6615.
(37) (a) Gorelsky, S. I.; *AOMix*, Program for Molecular Orbital Analysis, version 6.85, 2015; http://www.sg-chem.net/. (b) Gorelsky, S. I.; Lever, A. B. P. *J. Organomet. Chem.* **2001**, *635*, 187.
(38) Yamaguchi, K.; Fukui, H.; Fueno, T. *Chem. Lett.* **1986**, *15*, 625.

DOI: 10.1021/jacs.6b07716
J. Am. Chem. Soc. 2016, 138, 15917−15926